PAPER

Preparation and characterization of CNT films/silicone rubber composite with improved microwave absorption performance

IOP ebooks™

Bringing you innovative digital publishing with leading voices to create your essential collection of books in STEM research.

Start exploring the collection - download the first chapter of every title for free.

Materials Research Express

PAPER

Preparation and characterization of CNT films/silicone rubber composite with improved microwave absorption performance

Junyao Shen[1], Yongtao Yao[1], Yanju Liu[2] and Jinsong Leng[1]

[1] National Key Laboratory of Science and Technology on Advanced Composites in Special Environments, Harbin Institute of Technology, Harbin, People's Republic of China
[2] Department of Astronautical Science and Mechanics, Harbin Institute of Technology, Harbin, People's Republic of China

E-mail: lengjs@hit.edu.cn

Abstract

Fabrications of CNT films/SR and CNT powders/SR composites are introduced to provide the rational comparisons of their thermal, mechanical and electrical properties in this work. The growth of CNT films is firstly prepared with floating catalyst chemical vapor deposition (FCCVD) method. CNT films belong to multi-walled CNT and mesoporous characteristic by Raman and nitrogen adsorption-desorption measurements, respectively. CNT films/SR composite also presents better microwave absorption performances with the low-level CNT loadings (0.5 wt%), compared to the CNT powders/SR composites. It exhibits the minimum reflection loss (RL_{min}) of the CNT films/SR composite is -26.55 dB and related effective absorption bandwidth (RL < -10 dB) of 3.57 GHz (12.24–15.81 GHz) with 1 mm thickness. A proposed absorption mechanism is attributed to optimized impedance matching and enhanced conductive/dielectric losses in the CNT films/SR absorber.

1. Introduction

To date, electromagnetic (EM) pollutions are becoming a crucial issue with the high-speed development of information technology [1–3]. Like a global pandemic, it strongly affects both human healthy and regular functionalities of communication electronics [4–7]. In response to this problem, exploring carbon nanotube (CNT)-based microwave absorbers (MAs) become a hot spot in this field. Because CNT is eligible to an ideal MAs with its natural material characteristics of low density, high electrical conductivity, and high specific surface area [8–11]. CNT plays a role as the conductive filler to adjust permittivity of CNT/polymer composite for satisfying the required bandwidth absorption such as X-band [10–12]. However, the dilemma of CNT dosage is a roadblock to wild utilization of powder-like CNT in the CNT-based composite MAs. Specifically, it disturbs impedance matching condition to damage electromagnetic wave receiving-ability in the MAs with high CNT content. It has been observed that such MAs with very high CNT-loaded present strong surface reflection and low microwave absorption [13]. Oppositely, it is apt to CNT agglomeration in the low CNT-loading MAs, which hinders the formation of continuous networks for both dielectric and conductive losses [14, 15].

Concerning the choice of the polymer matrix, silicone rubber (SR), as a widely accepted polymer for novel stretchable electronics, is acceptable in this work. Because it has many merits like good elasticity with a large deformation [16, 17], biocompatibility [18, 19], acid/basic inertness [20] and excellent processability for molding [18, 21]. Sufficient CNT contents are in favor of conductive loss with forming microcurrent networks, which has been proved in other CNT-containing absorbers [8, 22]. It reports that even a 5 wt% CNT loading cannot help the RL values of CNT/SR absorber to reach the range of RL < -10 dB [23]. Using other second conductive phase is a resigned choice to amend the loss ability in the CNT/SR absorbers [23, 24]. It is still a challenge for improving microwave absorption in CNT/SR composite absorbers with low CNT content.

Table 1. The Contents and types of CNTs loading in the CNT/SR composites.

Sample	CNT contents (wt%)	CNT types	Mass (g)	
			CNT	SR precursor
Pure SR	0	—	0	20.62
0.5 CNT powders/SR	0.5	Powder	1.03	20.62
2.5 CNT powders/SR	2.5	Powder	5.15	20.62
0.5 CNT films/SR	0.5	Film	1.03	20.62

Recently, two-dimensional (2D) macroscopic CNT assemblies such as CNT films open up an alternative strategy to solve poor CNT dispersion and low EM wave absorption in CNT-containing composites [25–27]. Integrality of 2D CNT films will greatly reduce the susceptibility of CNT agglomeration into the polymer matrix and produce massive interfaces between CNT and polymer matrix to supply extra interfacial polarizations for dielectric loss [28]. Another merit of CNT films is accelerating the transport of charge carriers for Maxwell-Wagner-Sillars polarizations due to adjustable pore channels [29, 30]. However, the in-depth exploration is limited to study microwave absorption performances in CNT films/SR composites.

This work, CNT films are firstly grown by floating catalyst chemical vapor deposition (FCCVD) method before the fabrication of CNT films/SR composite with low CNT loadings (0.5 wt%) for characterization. The CNT powders/SR composites are also prepared for a rational comparison. As a case, both enhanced reflection loss and effective absorption bandwidth (RL $<$ -10 dB) can be found in the CNT films/SR composite for EM absorption performances. While the CNT powders/SR composites present much inferior reflection losses and no ranges of the effective absorption bandwidth under 1 mm coating thickness.

2. Experimental

2.1. Direct growth of CNT films
For the first step of CNT films growth, ethanol as liquid carbon source and ferrocene as growth activator with thiophene promoter-assisted were applied at 1150 °C via floating catalytic chemical vapor deposition approach [31]. The details were provided in the supplementary material.

For comparison, standard commercial CNT powders were purchased from Chengdu Organic Chemicals Co., Ltd Outer diameter of the commercial CNT powders is 8 nm and the related specific surface area is 110 $m^2 g^{-1}$.

2.2. Fabrication of CNT/SR composites
The pure SR laminate was prepared as our group previously reported [19, 32]. Typically, liquid SR precursor was configured with 15 g raw silicone rubber, 1.5 g curing agent and 4.12 g plasticizer (TC5005 A-B/C, BJB Enterprises Inc.). The mixture was poured into a sealing tank of the hybrid mixer (ARE-500, THINKY Inc., Japan). After mixing and degassing procedures, pure SR was molded as 1 mm thickness laminate and sequentially cured overnight under ambient temperature.

Preparation of CNT powders/SR composites was similar to that of pure SR laminate with the supplement of CNT powders as the fillers. The CNT powders were directly added into liquid SR precursor with two designated contents of CNT powders (0.5 wt% and 2.5 wt%). They were labeled as 0.5 CNT powders/SR and 2.5 CNT powders/SR, respectively. A substituted process was adopted to avoid damaging CNT films, which depicted that homogeneous liquid SR was dropwise infiltrated into CNT films in vacuum. The mass ratio of CNT films was 0.5 wt% in CNT films/SR composite, which is equal to 0.5 CNT powders/Sr It was named as 0.5 CNT films/SR. table 1 presents the detailed parameters in the CNT/SR composites.

2.3. Characterization
X-ray diffraction patterns of CNT films, pure SR and CNT/SR composites were determined from 20° to 60° with a spectrometer of X'PERT PRO MPD type (Cu Kα radiation; $\lambda = 0.154$ nm). Surface micro-morphologies of the samples were observed by a field-emission scanning electron microscopy (FESEM) with FEI Quanta 200 F type. The FESEM operation voltage is 20 KV. Thermo gravimetric analysis (TGA) was conducted to measure thermal stability of the CNT/SR composites. The testing temperature was from ambient temperature to 800 °C under airflow. A Q100 differential scanning calorimetric (DSC) analyzer (TA Instruments, USA) was also measured for the melting temperature of the CNT/SR composites. The heating rate was 10 °C min^{-1} for thermal measurements. Types and crystallized degree of CNT films were carried out via Raman spectroscopy. A Spectrum-Two type spectrometer (PerkinElmer Inc, USA) was used to record the Fourier transform infrared
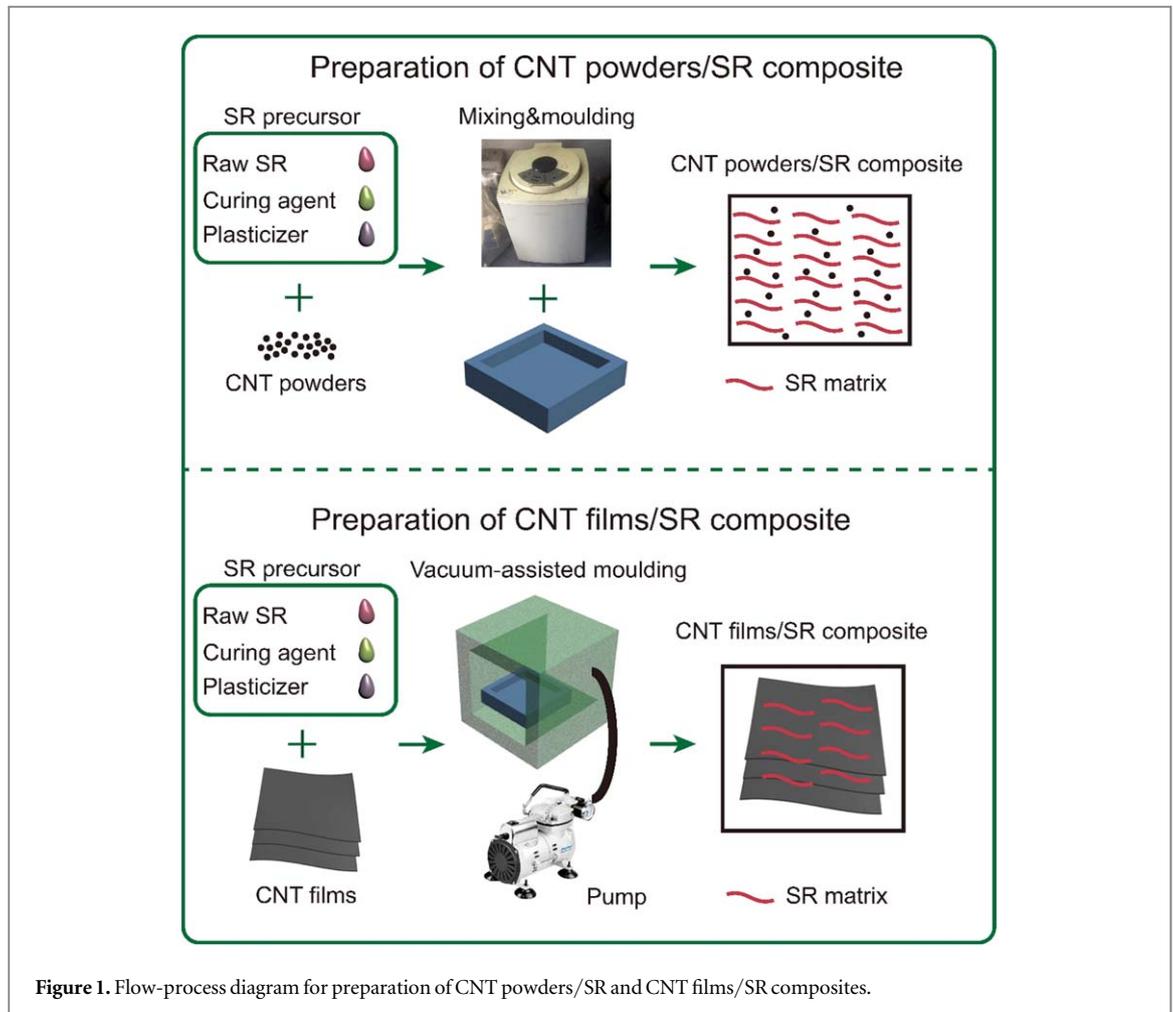
Figure 1. Flow-process diagram for preparation of CNT powders/SR and CNT films/SR composites.

spectroscopy (FTIR) data of the samples. Micromeritics ASAP 2020 system is applied for measuring specific surface area and the pore size distribution (BJH method) of CNT films by nitrogen adsorption-desorption isotherms. The mechanical properties of specimens were measured using a universal tensile testing machine (Z050, Zwick/Roell, Germany), which is according to the ASTM D638 standard. A sheet resistivity tester was applied to measure electrical resistivity by the four-point probe method (RT-70V, Napson, Japan). Electromagnetic parameters of SR/CNT composites were obtained from the N5234A-typed vector network analyzer. The reflection loss (RL) values of composite specimens, under different coating thickness of 1–2 mm, can be ascribed to the following equations [33, 34]:

$$Z = (\mu_r/\varepsilon_r)^{1/2}\tanh[j(2\pi f d)(\mu_r\varepsilon_r)^{1/2}/c] \tag{1}$$

$$RL = -20\log|(Z-1)/(Z+1)| \tag{2}$$

Where ε_r and μ_r are the relative complex permittivity and permeability of the absorbers. f represents the frequency of incident EM wave. d and c are coating thickness of the absorbers and the velocity of light in vacuum, respectively. Z is the normalized input impedance.

3. Results and discussion

3.1. Characterization of CNT films and CNT/SR composites

The growth of CNT films was firstly prepared through a horizontally placed furnace while the compared CNT powders were directly used without any further purification. Figure 1 presents the following processes for fabrication of CNT powders/SR and CNT films/SR composites, being fully considered with the difference macroscopic structures between CNT powders and CNT films.

Figure 2 presents the Raman spectrums of as-obtained CNT films and commercial CNT powders, as being a first glance to check the wall numbers and crystallized integrity of CNT. Due to being free of radial breathing mode (RBM) peaks [35] which demonstrate the existence of single-walled CNTs (SWNTs), it indicates that both CNT films and CNT powders are multi-walled carbon nanotubes (MWNTs). The D band (1350 cm^{-1})
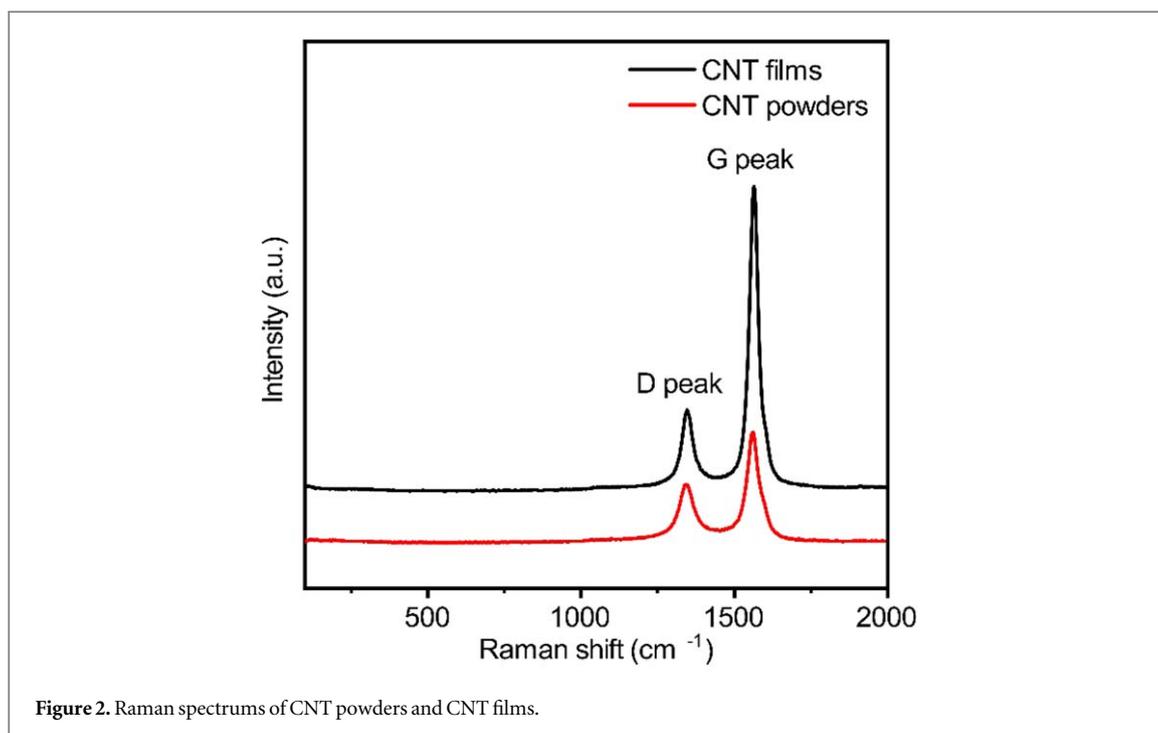
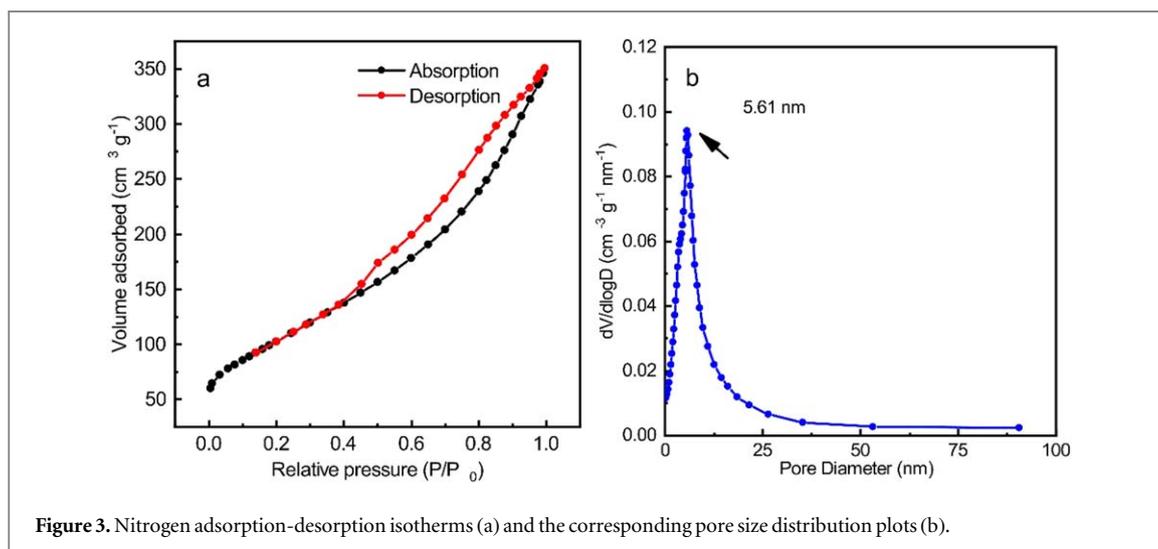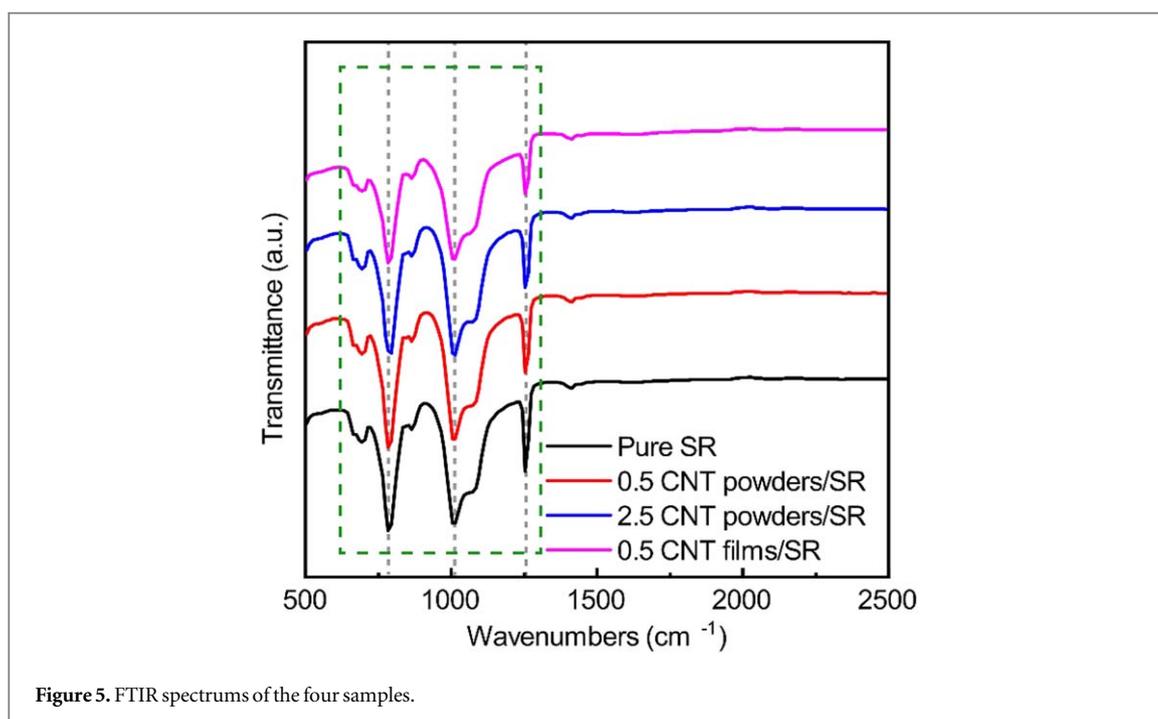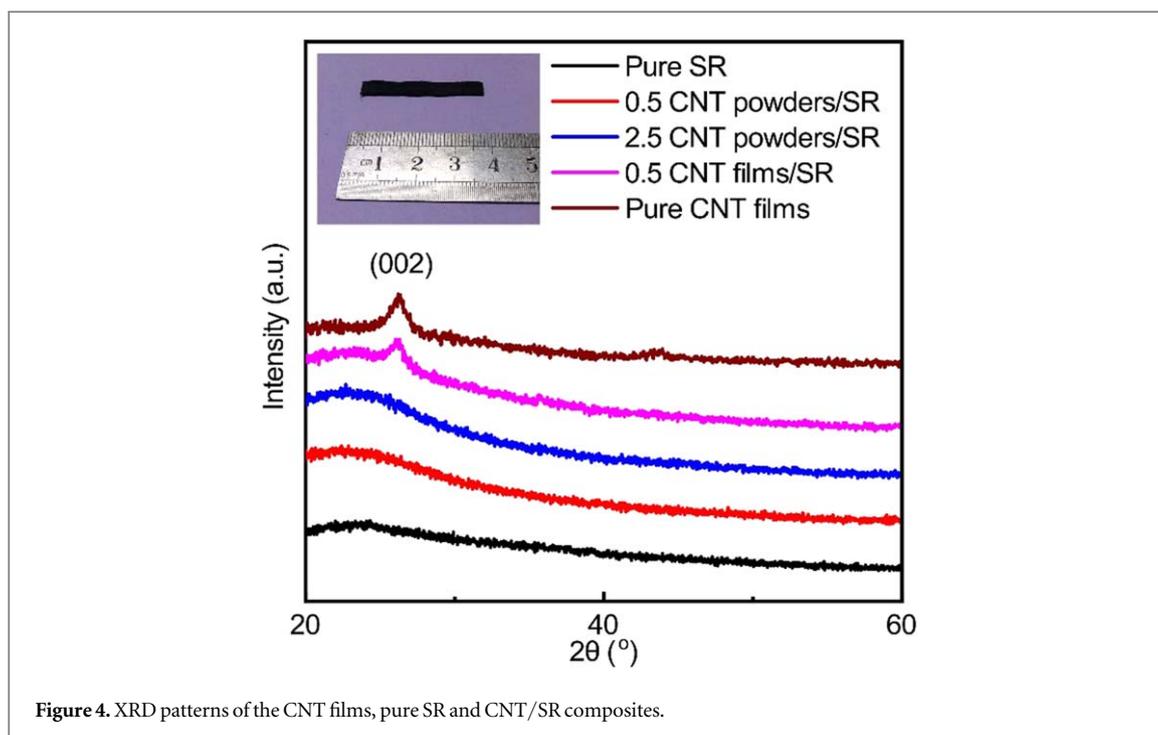**Figure 2.** Raman spectrums of CNT powders and CNT films.

Figure 3. Nitrogen adsorption-desorption isotherms (a) and the corresponding pore size distribution plots (b).

represents the degree of disorder in the in-plane graphite, while the G band (1580 cm^{-1}) reflects well-ordered graphite sheet with C–C vibrational mode [36–38]. It is widely accepted that ratio between the intensities of the G and the D bands (I_G/I_D) implies for the integrity of nanotube walls and crystallology perfection. The I_G/I_D ratio of CNT films is 3.62, which is much higher than the one of CNT powders (1.83). It reveals fewer amorphous carbon impurity and better crystallinity in the CNT films.
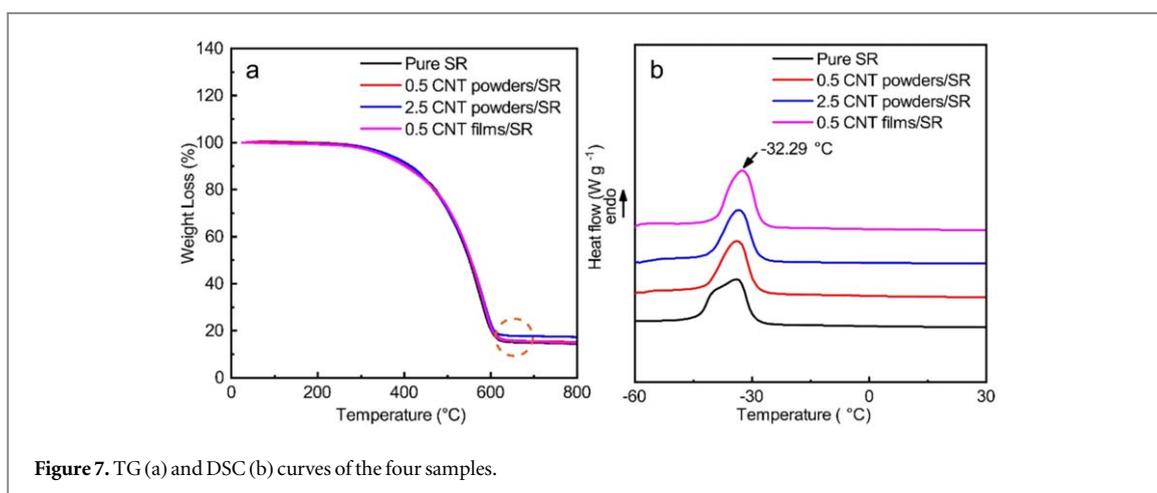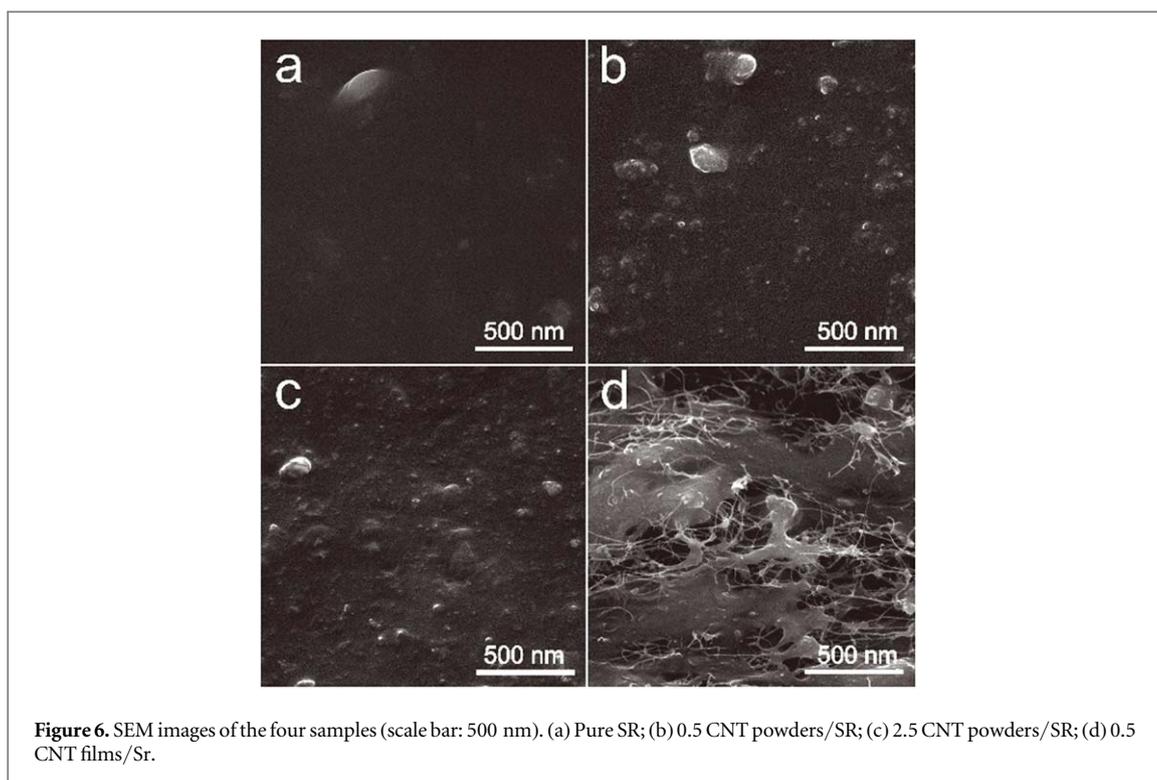
Figure 3 displays the Brunauer-Emmett-Teller (BET) specific surface area and the related pore size distribution of the CNT films since they possess the porous structure. The specific surface area of CNT films is 371.31 m^2 g^{-1} with a perfect closed loop containing the absorption/desorption curves. The CNT films also have a narrow pore size distribution with the intensity peak of 5.61 nm, which demonstrate the uniformly mesoporous characteristics.

Figure 4 shows structures of as-obtained CNT films and four CNT/SR composites via XRD patterns. The characteristic (002) peak of CNT films locates at 26.3° and d value is 0.34 nm, infering turbostratic graphene layer spacing of MWNTs [39, 40]. The inset displays the optical image of segmental original CNT films. The main characteristic peak is weak in pure SR with a poor crystalline nature in pure SR laminate and no CNT-featured peak is found in the CNT powders/SR composites (0.5 CNT powders/SR and 2.5 CNT powders/SR). The reason is that featured peak of thick SR matrix covering the one of CNT with very low content of CNT

Figure 4. XRD patterns of the CNT films, pure SR and CNT/SR composites.

Figure 5. FTIR spectrums of the four samples.

powders, making XRD analysis insensitive. However, due to enhancing the long-range order of film-like macrostructures, the featured (002) peak of CNT films is also observed in 0.5 CNT films/Sr.

FTIR spectrums further present the combination between CNTs and SR matrix with inspecting the distributions of silicon-containing groups (figure 5). The intrinsic functional groups of SR can be easily found in all the samples in the green dotted pane. It includes the peaks of Si–O–Si stretching for 1080 cm^{-1}, Si–O of O–Si(CH$_3$)$_2$–O for 790 cm^{-1} Si–CH$_3$ symmetric bending for 1260 cm^{-1}. Compare to the ones of Pure SR, the intensities of FTIR peaks are lowering with more CNTs adding in the CNT powders/SR composites. The reason might be attributed to steric hindrance of CNT to partially interrupt the Si-containing chemical bonds of SR for FTIR checking. It works on 0.5 CNT films/SR strongly, which presents the minimum FTIR peaks. Nevertheless, it is free of new chemical bondings between CNT and SR with no shifts of the featured peaks, according to the physical association processes for fabrication of the CNT/SR composites.

Figure 6. SEM images of the four samples (scale bar: 500 nm). (a) Pure SR; (b) 0.5 CNT powders/SR; (c) 2.5 CNT powders/SR; (d) 0.5 CNT films/Sr.

Figure 7. TG (a) and DSC (b) curves of the four samples.

The micromorphologies of four samples are detected with SEM characterization (figure 6). The luminous spotted CNT powders embed into the SR matrix with slight agglomeration in the CNT powders/SR composites (figures 6(b)–(c)), being similar to other reports [41, 42]. Meantime, it exhibits the spider-web-like CNT films entangled with the SR matrix in 0.5 CNT films/SR due to the macrostructures of CNT films (figure 6(d)).

TGA curves of these four samples display similar changes in total weight loss (figure 7(a)). Main weight loss is observed in the temperature region in 200 °C–600 °C. It is ascribed to thermal decomposition of both SR matrix and CNT. Equally low-level CNT contents are found in 0.5 CNT powders/SR and 0.5 CNT films/SR which is obeyed the design of experiments, marked at the selected circle area (See figure S1 is available online at stacks. iop.org/MRX/6/075610/mmedia). Different melting temperature (T_m) of the four samples is further measured by DSC curves (see figure 7(b)). Compared to other three samples, It presents the maximum featured endotherm peak in 0.5 CNT films/SR with T_m of −32.29 °C. Being different from powder-like CNTs, CNT films act as highly porous nets to separate SR matrix into the smaller units for retarding SR mobility, promoting the higher T_m in 0.5 CNT films/Sr We infer the changes in the mechanical properties of CNT/SR composites might also be happened due to the macrostructure between CNT powders and CNT films.

Figure 8 shows the stress-strain curves in the four samples. The tensile strength of 0.5 CNT films/SR is 1.02 MPa, which is higher than that of 0.5 CNT powders/SR with the value of 0.64 MPa under same CNT content adding (0.5 wt%). Fracture elongation of 0.5 CNT films/SR is the minimum among the four samples
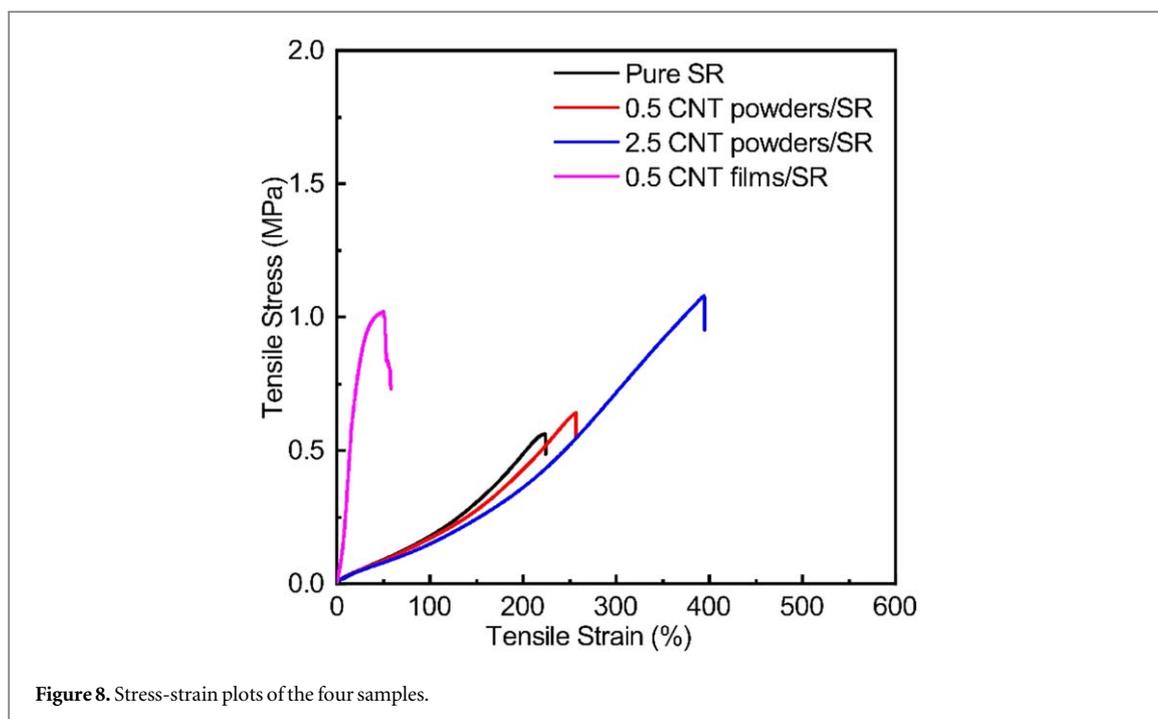
Figure 8. Stress-strain plots of the four samples.

due to a big gap of intrinsic strains between CNT films and SR matrix. However, it is still improved with complementarity from durability of SR matrix, compared to the ones of other pure 2D microstructured CNT assemblies [43, 44]. More details of mechanical properties can be found in table S1 (See the supplementary material).

Figure S2 presents pure SR, 0.5 CNT powders/SR, 2.5 CNT powders/SR and 0.5 CNT films/SR from left to right in the supplementary material (See the supplementary material). To better presentation, a strip of pure SR is maintained to distinguish the interface of CNT/SR-4 composite and pure SR as marked at the selected white area. Generally, pure SR is considered as a kind of insulation polymer matrix with a large electrical resistivity of 10^{14}–10^{16} Ω cm [41, 45, 46]. To reduce the electrical resistivities of CNT/SR composites are limited under a low-level of CNT powders adding (see Table S2). Electrical resistivities of the former three laminates fail to be measured due to the limitation of the measurement range of the resistivity tester. Meantime, electrical resistivity of 0.5 CNT films/SR is 2×10^{4} Ω cm, which might be benign to bulid interconnected microcurrent networks for the conductive loss.

3.2. Microwave absorption performance

The normalized input impedance Z is primarily crucial in the microwave absorption properties due to it represents impedance matching between free space and surface of the absorber, being expressed as equation (3). Figure 9 presents the changes of Z in the three CNT/SR composites absorbers. Ideally, the condition is $Z = 1$ for absolutely entering the interior of absorber [10, 47, 48]. The Z values of 0.5 CNT films/SR are very closely the ideal value of 1 in the range of 14.54–16.93 GHz, revealing the greatly enhanced impedance matching in this frequency range. While the Z values of the other two CNT powders/SR absorbers are much lower than the ones of 0.5 CNT films/SR in the range of 12–18 GHz, which is harmful to microwave absorption.

In practical demands of EM wave absorbers, the bandwidth of RL < -10 dB (here be denoted as f_E) exhibits that the absorbers have the ability of assimilating 90 % incident electromagnetic wave in the appointed bandwidth. It is widely accepted that f_E is one important index for evaluation of EM wave absorption, which is equal with the intensity index as the minimum reflection loss (RL_{min}) [5, 7, 49–51]. Figure 10(a) presents frequency bandwidth and intensity of the three CNT/SR absorbers (0.5 CNT powders/SR, 2.5 CNT powders/SR and 0.5 CNT films/SR) in RL curves at 1 mm coating thickness. It reveals that 0.5 CNT films/SR owns broader f_E and higher RLmin value than other two CNT powders/SR absorbers (0.5 CNT powders/SR and 2.5 CNT powders/SR). In detail, f_E of 0.5 CNT films/SR is up to 3.57 GHz (12.24–15.81 GHz) and the RLmin peak locates at 13.84 GHz with RLmin of -26.55 dB, presenting good electromagnetic absorption property. While the CNT powders/SR absorbers show much inferior values of RLmin peaks (0.5 CNT powders/SR: -3.90 dB; 0.5 CNT powders/SR: -6.00 dB) and both fail to reach the range of f_E. Figure 10(b) shows the contour map of absorption bandwidth in 0.5 CNT films/SR from 1 mm to 2 mm coating thickness, suggesting enlarged f_E of 9.73 GHz (6.08–15.81 GHz) in 0.5 CNT films/Sr Due to the facts of dielectric and conductivity loss dominating EM wave absorption in CNT filler-based polymer absorbers, it is of the importance to investigate on variation of
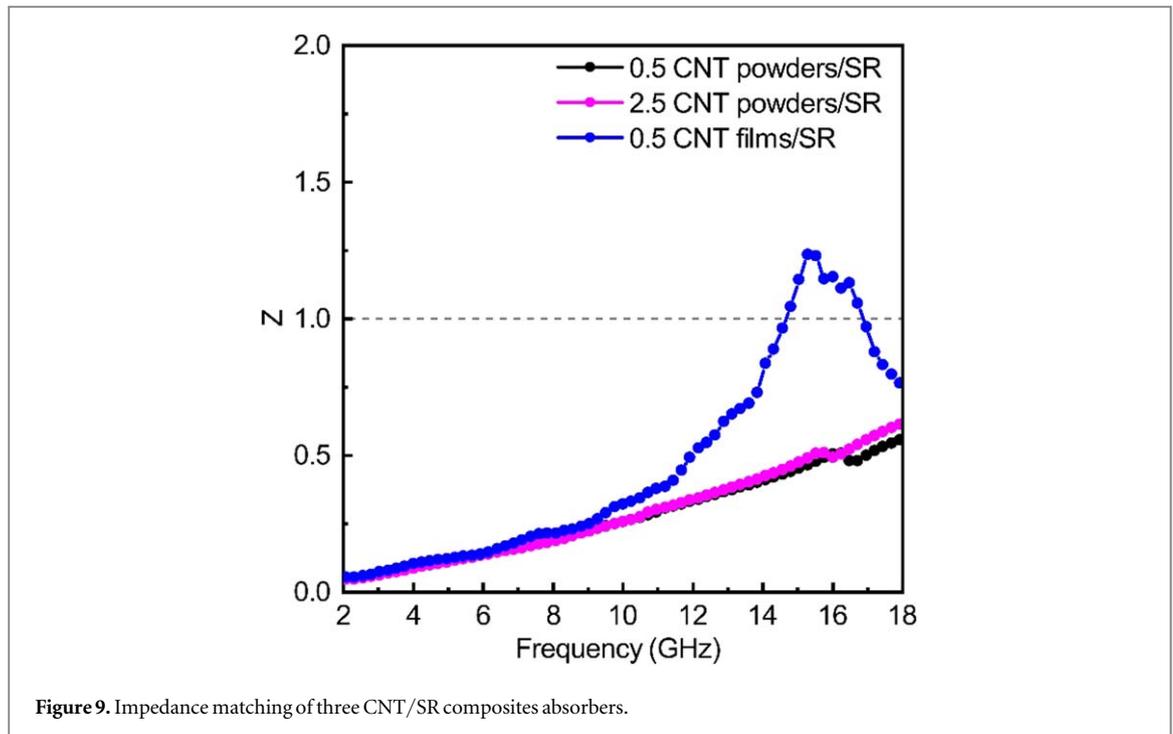
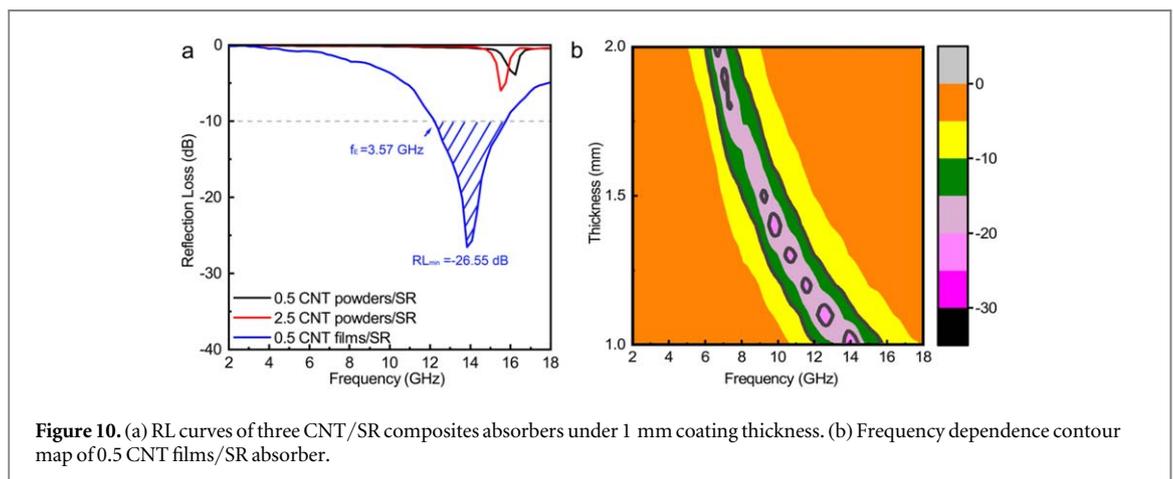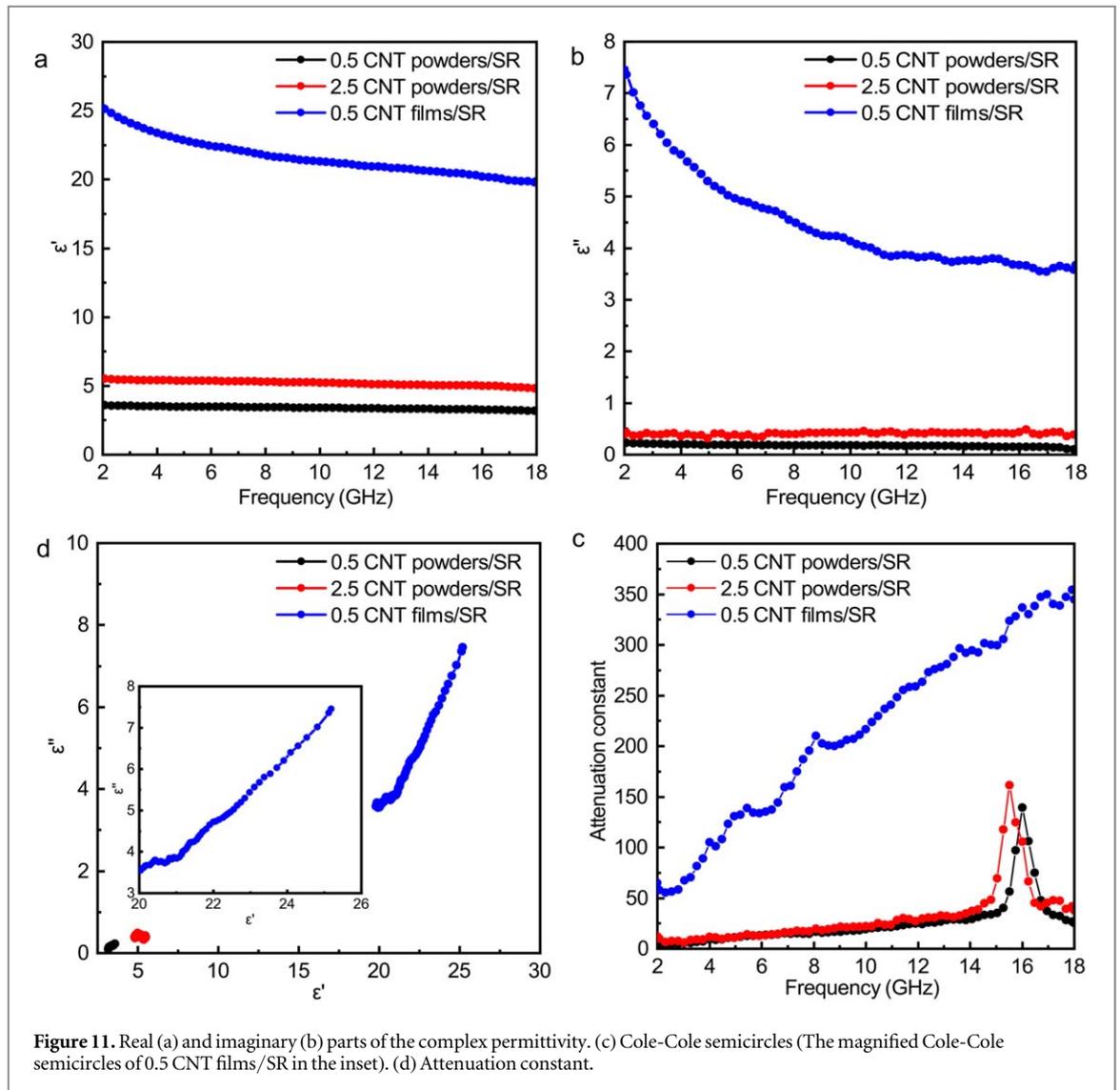**Figure 9.** Impedance matching of three CNT/SR composites absorbers.

Figure 10. (a) RL curves of three CNT/SR composites absorbers under 1 mm coating thickness. (b) Frequency dependence contour map of 0.5 CNT films/SR absorber.

complex permittivity ($\varepsilon_\gamma = \varepsilon' - j\varepsilon''$) in CNT/SR composites absorbers. Figures 11(a)–(b) presents details on real (ε') and imaginary (ε'') parts of complex permittivity (ε_r) in the three CNT/SR absorbers. ε' of 0.5 CNT films/SR present a several-fold improvement to those of CNT powders/SR absorbers. Real part permittivity (ε') of 0.5 CNT films/SR steadily decreases from 25.12 to 19.80, while those of CNT/SR-2 and CNT/SR-3 are almost constant with the end values of 3.17 and 4.80, respectively. As for the changes on ε'', ε'' of 0.5 CNT films/ SR sharply decrease in the first stage from 2–9.04 GHz and gradually stabilize in rest frequency range of 9.04–18 GHz, presenting the value from 7.36 to 3.58. While those of CNT powders/SR absorbers are constant with negligible values (0.5 CNT powders/SR: 0.09; 2.5 CNT powders/SR: 0.38) in the end of measurement frequency. ε'' of 0.5 CNT films/SR is still the highest in all of three CNT/SR composites absorbers. Generally, ε' represents storage ability of electromagnetic wave for microwave absorber and ε'' shows related dissipation ability [51, 52]. It has been evidenced that sufficient conductive networks from moderate improvement of ε' and ε'' contribute to improve microwave absorption on novel carbon-based multiphase absorbers [9, 10, 13]. The results are also be speculated that the higher ε'' of 0.5 CNT films/SR indicates a lower electrical resistivity, to finally obtain high conductivity according to the free electron theory ($\varepsilon'' = 1/2\pi\varepsilon_0\rho f$) [53, 54]. Higher ε'' values also have a positive effect on shrinkage of the gap between ε' and ε'' to obtain better impedance matching which has been proved in the Z results. Thus, the moderate permittivity is mainly in charge of optimizing the absorbing ability of EM wave in 0.5 CNT films/Sr.

Further the relationship of ε' and ε'' can be represented by plotting of ε' versus ε'', which is marked as Cole–Cole semicircles in figure 11(c). It represents Debye dipolar relaxations for prompted dielectric loss in EM

Figure 11. Real (a) and imaginary (b) parts of the complex permittivity. (c) Cole-Cole semicircles (The magnified Cole-Cole semicircles of 0.5 CNT films/SR in the inset). (d) Attenuation constant.

absorption. Each Debye relaxation process corresponds to one semicircle in the profiles of Cole–Cole semicircles, being depicted as following equations: [23, 55]

$$\varepsilon' = \varepsilon_\infty + \frac{\varepsilon_s - \varepsilon_\infty}{1 + (2\pi f)^2 \tau^2} \tag{3}$$

$$\varepsilon'' = \frac{2\pi f \tau (\varepsilon_s - \varepsilon_\infty)}{1 + (2\pi f)^2 \tau^2} \tag{4}$$

$$\varepsilon_r = \varepsilon' + i\varepsilon'' = \varepsilon_\infty + \frac{\varepsilon_s - \varepsilon_\infty}{1 + j2\pi f\tau} \tag{5}$$

$$(\varepsilon' - \varepsilon_\infty)^2 + (\varepsilon'')^2 = (\varepsilon_s - \varepsilon_\infty)^2 \tag{6}$$

Where ε_s and ε_∞ are the static permittivity and infinite dielectric constant, and τ represents relaxation time. Multiple Cole-Cole semicircles are easily found in the inset of figure 11(c), showing multiple Debye dipolar relaxations for the contribution of permittivity dispersion in 0.5 CNT films/Sr Meanwhile, those of CNT powders/SR absorbers present worm-like short plots of ε' versus ε'' near the origin of coordinates, showing inferior effects on permittivity dispersion with less Cole-Cole polarization relaxation processes. Another useful tool is denoted as attenuation constant (α) to evaluate the internal microwave attenuation of absorber, being described as the following equation: [48, 56]

$$\alpha = \sqrt{2}\pi f \times c^{-1} \times [(\mu''\varepsilon'' - \mu'\varepsilon') + \sqrt{(\mu''\varepsilon'' - \mu'\varepsilon')^2 + (\varepsilon'\mu'' + \varepsilon''\mu')^2}]^{1/2} \tag{7}$$

Figure 11(d) presents that all α values of 0.5 CNT films/SR are higher than those of other two CNT powders/SR absorbers in whole measurement frequency of 2–18 GHz. While those of 0.5 CNT powders/SR and 2.5 CNT powders/SR are negilibile in major fequency range expect for an obvious fluctuation with a range of
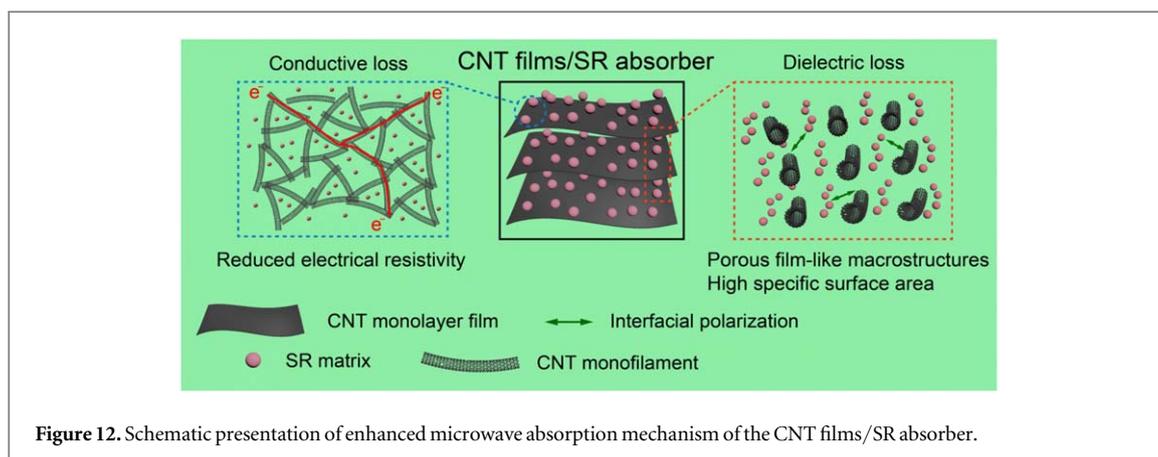
Figure 12. Schematic presentation of enhanced microwave absorption mechanism of the CNT films/SR absorber.

14.80–16.96 GHz, being well consitient with RL results in figure 10. It reveals that better EM wave attenuation in the interior of 0.5 CNT films/SR than ones of 0.5 CNT powders/SR and 2.5 CNT powders/Sr We infer that 2D CNT films supplies fully developed microcurrent networks as another key role to the contribution of conductive loss for microwave attenuation besides as-mentioned dielectric loss.

Figure 12 exhibits the schematic illustration of possible improved microwave absorption in the CNT films/ SR absobers. The integrity of CNT films is favor of enhancing conductive loss with effeicently interconnected microcurrent networks in the CNT films/SR absorber, being consitent to the largely reduced electrical resistivity with a low-level CNT loadings (0.5 wt%). The second contributor is attributed to the enhanced dielectric loss with multi-polarization processes which mainly originates from Debye dipolar relaxation and interfacial polarization. The mesoporous nature of CNT films give efficient nanosized effect for multi-polarization. Also, the higher BET surface area (371.31 $m^2\,g^{-1}$) of CNT films provide abounding interfaces between CNT films and SR matrix for generating interfacial polarization in the CNT films/SR absorber. Eventually, the promotion of conductive/dielectric losses and balanced impedance matching are responsible for improving microwave absorption performance of the CNT films/SR composite absorber.

4. Conclusions

In summary, we have prepared CNT films by CVD approach and subsequently fabricated CNT films/SR composite for characterization and related EM wave absorption performances. Being the film-like macrostructure, CNT films greatly influence the thermal, mechanical, electrical, and microwave absorption properties. For example, The CNT films/SR composite show improved T_m ($-32.29\ ^\circ C$) and tensile strength (1.02 MPa). Electrical resistivity of the CNT films/SR composite reduces to the value of $2 \times 10^4\,\Omega$ cm, while those of CNT powders/SR composites perform insulated. The CNT films/SR composite also presents good microwave absorption with the R_{min} of -26.55 dB and the efficient bandwidth of 3.57 GHz due to good impedance matching and enhanced conductive/dielectric losses. We hope some value results from this work are available to the guidance of novel CNT-based MAs in the future.

Acknowledgments

ORCID iDs

Yanju Liu ⓘ https://orcid.org/0000-0001-8269-1594
Jinsong Leng ⓘ https://orcid.org/0000-0001-5098-9871

References

[1] Motmaen D, Kianvash A and Shokrvash H 2018 An investigation into microwave absorption properties of carbonyl iron/La$_{0.7}$Sr$_{0.3}$Mn$_{1-x}$Co$_x$O$_3$ (x = 0, 0.2, 0.4, 0.6, 0.8) nanocomposites *Mater. Res. Express* **5** 086107

[2] Shi X F, Liu Z W, You W B, Zhao X B and Che R C 2018 Janus-like Fe_3O_4/PDA vesicles with broadening microwave absorption bandwidth *Journal of Materials Chemistry C* **6** 7790–6

[3] Prasad J, Singh A K, Shah J, Kotnala R K and Singh K 2018 Synthesis of MoS_2-reduced graphene oxide/Fe_3O_4 nanocomposite for enhanced electromagnetic interference shielding effectiveness *Mater. Res. Express* **5** 055028

[4] Pervaiz E, Gul I H and Virk M S 2014 Magnetic and RF-electromagnetic absorbing study of aluminum doped nickel ferrites prepared by two techniques *Mater. Res. Express* **1** 016104

[5] Chen J B, Tan S J, Liang X H, Liu W and Ji G B 2019 Rod-like Te as excellent microwave absorber: a new exploration *J. Alloys Compd.* **777** 1197–203

[6] Shen J Y, Yao Y T, Liu Y J and Leng J S 2016 Tunable hierarchical Fe nanowires with a facile template-free approach for enhanced microwave absorption performance *J. Mater. Chem.* C **4** 7614–21

[7] Xu H L, Yin X W, Li M H, Ye F, Han M K, Hou Z X, Li X L, Zhang L T and Cheng L F 2018 Mesoporous carbon hollow microspheres with red blood cell like morphology for efficient microwave absorption at elevated temperature *Carbon* **132** 343–51

[8] Lv H L, Ji G B, Zhang H Q and Du Y W 2015 Facile synthesis of a CNT@Fe@SiO_2 ternary composite with enhanced microwave absorption performance *RSC Adv.* **5** 76836–43

[9] Ning M, Li J, Kuang B, Wang C, Su D, Zhao Y, Jin H and Cao M 2018 One-step fabrication of N-doped CNTs encapsulating M nanoparticles (M = Fe, Co, Ni) for efficient microwave absorption *Appl. Surf. Sci.* **447** 244–53

[10] Zhong B, Cheng Y J, Wang M, Bai Y Q, Huang X X, Yu Y L, Wang H T and Wen G W 2018 Three dimensional hexagonal boron nitride nanosheet/carbon nanotube composites with light weight and enhanced microwave absorption performance *Composites Part A: Applied Science and Manufacturing* **112** 515–24

[11] Kausar A, Rafique I and Muhammad B 2016 Review of applications of polymer/carbon nanotubes and epoxy/CNT composites *Polym.-Plast. Technol. Eng.* **55** 1167–91

[12] Tiwari D C, Dipak P, Dwivedi S K, Shami T C and Dwivedi P 2018 PPy/TiO_2(np)/CNT polymer nanocomposite material for microwave absorption *J. Mater. Sci., Mater. Electron.* **29** 1643–50

[13] Chen Y, Liu X, Mao X, Zhuang Q, Xie Z and Han Z 2014 γ-Fe_2O_3-MWNT/poly(p-phenylenebenzobisoxazole) composites with excellent microwave absorption performance and thermal stability *Nanoscale* **6** 6440–7

[14] Zhang X *et al* 2015 Electrically conductive polypropylene nanocomposites with negative permittivity at low carbon nanotube loading levels *ACS Applied Materials & Interfaces* **7** 6125–38

[15] Kaseem M, Hamad K and Ko Y G 2016 Fabrication and materials properties of polystyrene/carbon nanotube (PS/CNT) composites: a review *Eur. Polym. J.* **79** 36–62

[16] Liu L W, Liu Y J, Li B, Yang K, Li T F and Leng J S 2011 Thermo-electro-mechanical instability of dielectric elastomers *Smart Mater. Struct.* **20** 075004

[17] Liu L W, Liu Y J, Zhang Z, Li B and Leng J S 2010 Electromechanical stability of electro-active silicone filled with high permittivity particles undergoing large deformation *Smart Mater. Struct.* **19** 115025

[18] Kong J H, Tong Y J, Sun J T, Wei Y F, Thitsartarn W, Jayven C C Y, Muiruri J K, Wong S Y and He C B 2018 Electrically conductive PDMS-grafted CNTs-reinforced silicone elastomer *Compos. Sci. Technol.* **159** 208–15

[19] Lv X F, Liu L W, Liu Y J and Leng J S 2015 Dielectric elastomer energy harvesting: maximal converted energy, viscoelastic dissipation and a wave power generator *Smart Mater. Struct.* **24** 115036

[20] Swanson J W and Lebeau J E 1974 The effect of implantation on the physical properties of silicone rubber *J. Biomed. Mater. Res.* **8** 357–67

[21] Hu H Q, Zhao L, Liu J Q, Liu Y, Cheng J M, Luo J, Liang Y R, Tao Y, Wang X and Zhao J 2012 Enhanced dispersion of carbon nanotube in silicone rubber assisted by graphene *Polymer* **53** 3378–85

[22] Wen B, Cao M S, Hou Z L, Song W L, Zhang L, Lu M M, Jin H B, Fang X Y, Wang W Z and Yuan J 2013 Temperature dependent microwave attenuation behavior for carbon-nanotube/silica composites *Carbon* **65** 124–39

[23] Kong L, Yin X W, Yuan X Y, Zhang Y J, Liu X M, Cheng L F and Zhang L T 2014 Electromagnetic wave absorption properties of graphene modified with carbon nanotube/poly(dimethyl siloxane) composites *Carbon* **73** 185–93

[24] Xu Y G, Zhang D Y, Cai J, Yuan L M and Zhang W Q 2012 Effects of multi-walled carbon nanotubes on the electromagnetic absorbing characteristics of composites filled with carbonyl iron particles *Journal of Materials Science & Technology* 34–40

[25] Lee S H, Kang D and Oh I K 2017 Multilayered graphene-carbon nanotube-iron oxide three-dimensional heterostructure for flexible electromagnetic interference shielding film *Carbon* **111** 248–57

[26] Miao H Y, Liu J H and Saravanan L 2015 Fabrication of alumina filled hybrid buckypaper composites and their enhancement of microwave absorbing performance *J. Phys. D: Appl. Phys.* **48** 215301

[27] Sun H, Che R C, You X, Jiang Y S, Yang Z B, Deng J, Qiu L B and Peng H S 2014 Cross-stacking aligned carbon-nanotube films to tune microwave absorption frequencies and increase absorption intensities *Adv. Mater.* **26** 8120–5

[28] Mao F, Shi Z, Wang J, Zhang C, Yang C and Huang M 2018 Improved dielectric permittivity and retained low loss in layer-structured films via controlling interfaces *Advanced Composites and Hybrid Materials* **1** 548–57

[29] Quan B, Liang X H, Ji G B, Cheng Y, Liu W, Ma J N, Zhang Y N, Li D R and Xu G Y 2017 Dielectric polarization in electromagnetic wave absorption: review and perspective *J. Alloys Compd.* **728** 1065–75

[30] Yao S H, Yuan J K, Mehedi H-a, Gheeraert E and Sylvestre A 2017 Carbon nanotube forest based electrostatic capacitor with excellent dielectric performances *Carbon* **116** 648–54

[31] Xu X K, Zhang Y, Jiang J, Wang H, Zhao X L, Li Q W and Lu W B 2017 *In-situ* curing of glass fiber reinforced polymer composites via resistive heating of carbon nanotube films *Compos. Sci. Technol.* **149** 20–7

[32] Feng N, Liu L W, Liu Y J and Leng J S 2015 Characteristics of multi-functional composites using elastomer embedded with shape memory alloy wires *Mater. Des.* **88** 75–81

[33] Singh P, Babbar V K, Razdan A, Srivastava S L and Goel T C 2000 Microwave absorption studies of Ca–NiTi hexaferrite composites in X-band *Materials Science and Engineering:* B **78** 70–4

[34] Guo Z H, Park S, Hahn H T, Wei S Y, Moldovan M, Karki A B and Young D P 2007 Magnetic and electromagnetic evaluation of the magnetic nanoparticle filled polyurethane nanocomposites *J. Appl. Phys.* **101** 09M511

[35] Theodore M, Hosur M, Thomas J and Jeelani S 2011 Influence of functionalization on properties of MWCNT-epoxy nanocomposites *Materials Science and Engineering:* A **528** 1192–200

[36] Hanana M *et al* 2018 Synergic effect on oxygen reduction reaction of strapped iron porphyrins polymerized around carbon nanotubes *New J. Chem.* **42** 19749–54

[37] Kumar G S and Patro T U 2018 Efficient electromagnetic interference shielding and radar absorbing properties of ultrathin and flexible polymer-carbon nanotube composite films *Mater. Res. Express* **5** 115304

[38] Ko J, Jee S, Lee J H and Kim S H 2018 High durability conductive textile using MWCNT for motion sensing *Sensors and Actuators A: Physical* **274** 50–6

[39] Tripathi B, Srivastava N, Sharma K B, Zagorskiy D and Katiyar R S 2017 MWNT/Cellulose based nanocomposite electrodes for ultrafast flexible li-ion battery *Macromolecular Symposia* **376** 1700042

[40] Georgakilas V, Koutsioukis A, Petr M, Tucek J and Zboril R 2016 Remarkable enhancement of the electrical conductivity of carbon nanostructured thin films after compression *Nanoscale* **8** 11413–7

[41] Maghsoudi K, Momen G, Jafari R and Farzaneh M 2018 Direct replication of micro-nanostructures in the fabrication of superhydrophobic silicone rubber surfaces by compression molding *Appl. Surf. Sci.* **458** 619–28

[42] Li Y L, Li M J, Pang M L, Feng S Y, Zhang J and Zhang C Q 2015 Effects of multi-walled carbon nanotube structures on the electrical and mechanical properties of silicone rubber filled with multi-walled carbon nanotubes *J. Mater. Chem.* C **3** 5573–9

[43] Xia Q S, Zhang Z C, Chu H T, Liu Y J and Leng J S 2018 Research on high electromagnetic interference shielding effectiveness of a foldable buckypaper/polyacrylonitrile composite film via interface reinforcing *Composites Part A: Applied Science and Manufacturing* **113** 132–40

[44] Chen Y, Zhang L, Zhan H and Wang J N 2016 New processing method to fabricate high-performance carbon-nanotube/polyvinyl alcohol composite films *Carbon* **110** 490–6

[45] Song Y Z, Yu J H, Yu L H, Alam F E, Dai W, Li C Y and Jiang N 2015 Enhancing the thermal, electrical, and mechanical properties of silicone rubber by addition of graphene nanoplatelets *Mater. Des.* **88** 950–7

[46] Hidayah N, Mustapha M, Ismail H and Kamarol M 2017 Linear low-density polyethylene/silicone rubber nanocomposites *Journal of Elastomers & Plastics* **50** 36–57

[47] Wu Y, Shu R W, Li Z Y, Guo C L, Zhang G Y, Zhang J B and Li W J 2019 Design and electromagnetic wave absorption properties of reduced graphene oxide/multi-walled carbon nanotubes/nickel ferrite ternary nanocomposites *J. Alloys Compd.* **784** 887–96

[48] Wei H J, Yin X W, Li X, Li M H, Dang X L, Zhang L T and Cheng L F 2019 Controllable synthesis of defective carbon nanotubes/$Sc_2Si_2O_7$ ceramic with adjustable dielectric properties for broadband high-performance microwave absorption *Carbon* **147** 276–83

[49] Yan S J, Wang L N, Wang T H, Zhang L Q, Li Y F and Dai S L 2016 Synthesis and microwave absorption property of graphene oxide/ carbon nanotubes modified with cauliflower-like Fe_3O_4 nanospheres *Appl. Phys.* A **122** 235

[50] Shen J Y, Yao Y T, Liu Y J and Leng J S 2019 Amorphous bimetallic nanowires with high-performance microwave absorption: a case for FeCo nanowires *NANO* **14** 1950041

[51] Cheng Y, Cao J M, Lv H L, Zhao H Q, Zhao Y and Ji G B 2019 *In situ* regulating aspect ratio of bamboo-like CNTs via Co_xNi_{1-x}-catalyzed growth to pursue superior microwave attenuation in X-band *Inorganic Chemistry Frontiers* **6** 309–16

[52] Wang H G, Meng F B, Li J Y, Li T, Chen Z J, Luo H B and Zhou Z W 2018 Carbonized design of hierarchical porous carbon/Fe_3O_4@Fe derived from loofah sponge to achieve tunable high-performance microwave absorption *ACS Sustainable Chemistry & Engineering* **6** 11801–10

[53] Zhang X F, Dong X L, Huang H, Liu Y Y, Wang W N, Zhu X G, Lv B, Lei J P and Lee C G 2006 Microwave absorption properties of the carbon-coated nickel nanocapsules *Appl. Phys. Lett.* **89** 053115

[54] Yang L F, Cai H P, Zhang B, Huo S Q and Chen X 2018 Enhanced microwave absorption property of epoxy nanocomposites based on PANI@Fe_3O_4@CNFs nanoparticles with three-phase heterostructure *Mater. Res. Express* **5** 025304

[55] Zhang Y N, Zhang Xm, Quan B, Ji G B, Liang Xh, Liu W and Du Y W 2017 A facile self-template strategy for synthesizing 1D porous Ni@C nanorods towards efficient microwave absorption *Nanotechnology* **28** 115704

[56] Singh S K, Akhtar M J and Kar K K 2019 Impact of Al_2O_3, TiO_2, ZnO and $BaTiO_3$ on the microwave absorption properties of exfoliated graphite/epoxy composites at X-band frequencies *Composites Part B: Engineering* **167** 135–46